

# Supporting Information

## Correlating the Synthesis, Structure and Catalytic Performance of Pt-Re/TiO<sub>2</sub> for the Aqueous-Phase Hydrogenation of Carboxylic Acid Derivatives

*Moritz O. Haus<sup>1</sup>, Alexander Meledin<sup>2,3</sup>, Sebastian Leiting<sup>4</sup>, Yannik Louven<sup>1</sup>, Nico C. Roubicek<sup>1</sup>, Sven Moos<sup>1</sup>, Claudia Weidenthaler<sup>4</sup>, Thomas E. Weirich<sup>2</sup> and Regina Palkovits<sup>1,\*</sup>*

<sup>1</sup> Lehrstuhl für Heterogene Katalyse und Technische Chemie, RWTH Aachen University, Worringerweg 2, DE-52074 Aachen.

<sup>2</sup> Gemeinschaftslabor für Elektronenmikroskopie / Institut für Kristallographie, RWTH Aachen University, Ahornstraße 55, DE-52074, Aachen.

<sup>3</sup> Ernst Ruska-Centre for Microscopy and Spectroscopy with Electrons (ER-C), Forschungszentrum Jülich GmbH, DE-52428 Jülich

<sup>4</sup> Max-Planck-Institut für Kohlenforschung, Kaiser-Wilhelm-Platz 1, D-45470 Mülheim an der Ruhr.

\*E-Mail: [palkovits@itmc.rwth-aachen.de](mailto:palkovits@itmc.rwth-aachen.de)

## TABLE OF CONTENTS

1. Pre-Experiments for Pt-Re/TiO <sub>2</sub> (SEA) .....	3
2. Kinetic Analysis of Amidation-Hydrogenation over Pt-Re/TiO <sub>2</sub> (LD).....	5
3. Maximum Achievable Yield .....	6
4. Heterogeneous Nature of the Catalyst.....	7
5. CSTR Catalyst Testing (Supplement) .....	8
6. XRD Analysis (Supplement).....	9
7. TEM Analysis (Supplement).....	10
8. XPS Analysis (Supplement).....	14
9. CO-FTIR (Supplement).....	17
10. Solvent-Effect on HESim Reduction.....	18
11. Pressure-Dependence of HESim Hydrogenation .....	19
12. Dynamics of Pt-Re/TiO <sub>2</sub> Catalysts .....	20
13. Characterization of Spent Catalyst .....	21
14. REFERENCES .....	24

## 1. Pre-Experiments for Pt-Re/TiO<sub>2</sub> (SEA)

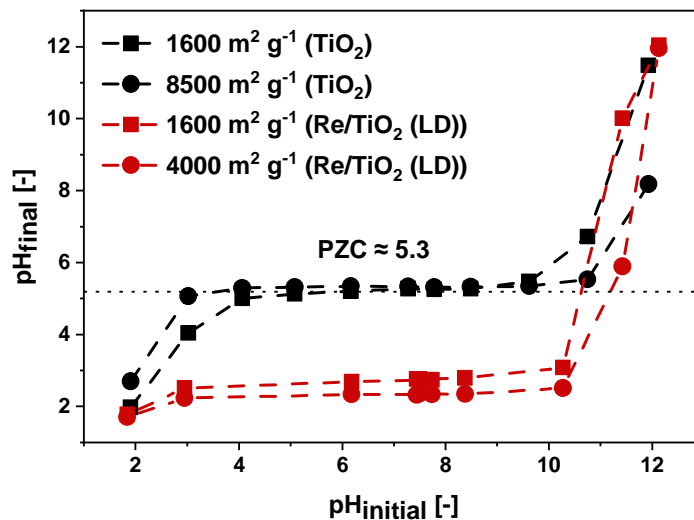


**Figure S1:** pH-shift curves recorded for the addition of ground TiO<sub>2</sub> (anatase, Saint-Gobain ST6\*120) and Re/TiO<sub>2</sub> (LD) to solutions of defined pH<sub>initial</sub>. (ionic strength = 0.1 mol L<sup>-1</sup> for all solutions, adjustment *via* the addition of NaNO<sub>3</sub>)

To conduct a controlled impregnation *via* the SEA (strong electrostatic adsorption) literature protocol, the PZC (point of zero charge) of the support material must be known. Fortunately, this value can be determined by monitoring the pH shift caused by the addition of support to solutions of defined initial pH.<sup>[1]</sup> In our experiments, we prepared aqueous solutions of NaOH and HNO<sub>3</sub> with defined initial pH values and adjusted them uniformly to an ionic strength of 0.1 mol L<sup>-1</sup> using NaNO<sub>3</sub>. Subsequently, a defined amount of ground TiO<sub>2</sub> (or Re/TiO<sub>2</sub> (LD)) was added to each of the thus prepared solutions, leading to a change in pH. The latter was recorded after the samples were equilibrated under continuous stirring. The resulting curves of pH<sub>initial</sub> vs pH<sub>final</sub> (**Figure S1**) exhibit clear plateaus in the intermediate pH range for TiO<sub>2</sub>. According to Park and Regalbuto<sup>[2]</sup> the corresponding values of pH<sub>final</sub> can serve as an estimate

for the oxide PZC. While this is not a precise method under all circumstances, the coincidence of plateaus obtained for different surface loadings ( $SSA_{TiO_2} V_{solution}^{-1}$ ) and their position in the intermediate pH range ( $pH_{PZC} \approx 5.3$ ) underline the estimate's validity. Notably, the obtained  $pH_{PZC}$  agrees well with literature sources.<sup>[3]</sup>

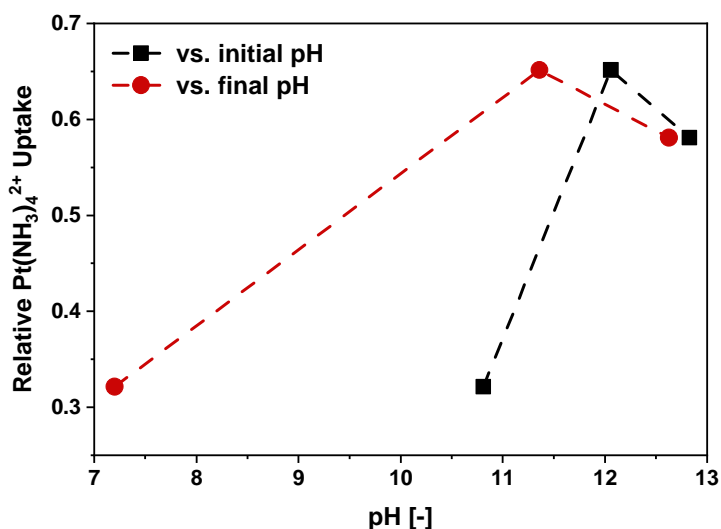


**Figure S2:** Pt-uptake vs. pH in the SEA impregnation of TiO<sub>2</sub>. The amount of precursor deposited on the support was determined via the remaining Pt(NH<sub>3</sub>)<sub>4</sub>(NO<sub>3</sub>)<sub>2</sub> concentration in the liquid after filtration (ICP-MS analysis). (Conditions: room temperature, 2000 m<sup>2</sup> L<sup>-1</sup>)

Given the  $pH_{PZC}$  of TiO<sub>2</sub> it follows that Pt impregnation will be most successful with positively charged complexes (e.g. Pt(NH<sub>3</sub>)<sub>4</sub><sup>2+</sup>) at basic pH values. These conditions will lead to the deprotonation of hydroxyl groups, causing a net negative charge on the TiO<sub>2</sub> surface. While the most optimal impregnation pH could be determined via modelling,<sup>[4]</sup> a small set of test experiments was chosen herein. In detail, the amount of Pt precursor that was removed from the impregnation solution due to its adsorption on TiO<sub>2</sub> was measured (ICP-MS) as a function of pH (**Figure S2**). The results indicate an optimal  $pH_{initial} \approx 12$ . Below that value, electronic

precursor-support interaction is reduced, whereas shielding effects dominate at higher pH. It is noted that Re/TiO<sub>2</sub> (LD) is characterized by a comparably strong acidic behavior in aqueous solution (Figure S1). Thus, even Pt impregnation without pH adjustment may be influenced by the strong electrostatic adsorption phenomenon.

## 2. Kinetic Analysis of Amidation-Hydrogenation over Pt-Re/TiO<sub>2</sub> (LD)

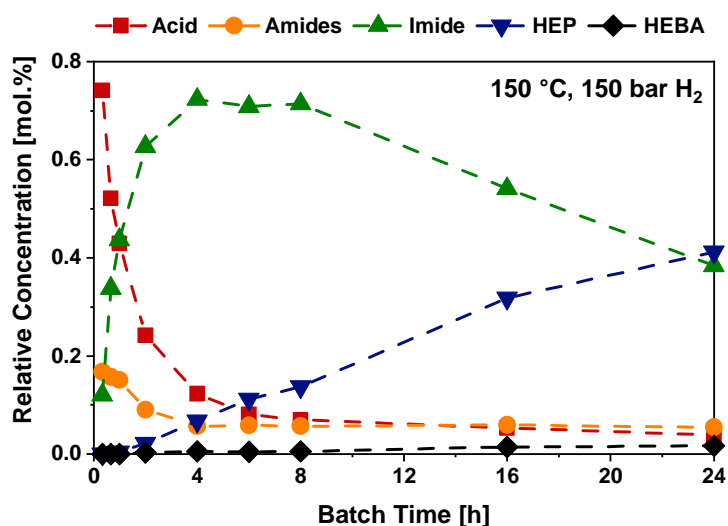


**Figure S3:** Concentration-time profile for the reductive transformation of succinic acid with ethanolamine over Pt-Re/TiO<sub>2</sub> (LD). (Conditions: 150 °C, 150 bar H<sub>2</sub>, 750 rpm, 1.5 g acid, 1.5 g H<sub>2</sub>O, 1 mol. equiv. amine, 37.5 mg catalyst)

A kinetic analysis of amidation-hydrogenation was previously shown for Ru/C.<sup>[5]</sup> The question remains, however, if the proposed reaction network (main text, Scheme 1) can be transferred to other catalytic systems. In this context, **Figure S3** shows the concentration-time profile of succinic acid amidation-hydrogenation over Pt-Re/TiO<sub>2</sub> (LD). Since the sequence of product

formation as well as the relative abundance of species are aligned with previous results, changes to the proposed reaction network are unnecessary. The hydrogenation of *N*-(2-hydroxyethyl)-succinimid to *N*-(2-hydroxyethyl)-2-pyrrolidone (HEP) and *N*-(2-hydroxyethyl)-4-hydroxybutanamide (HEBA) is thus established as rate-determining step.

### 3. Maximum Achievable Yield

**Table S1:** Detailed summary of reaction results with Ru/C and Pt-Re/TiO<sub>2</sub> (LD) at high conversion. (Conditions: 200 °C, 150 bar H<sub>2</sub>, 750 rpm, 24 h.)

Substrate/Product (i)	$n_i/n_{\text{substrate},0}$ [mol mol <sup>-1</sup> ]	
	Ru/C	Pt-Re/TiO <sub>2</sub> (LD)
Succinic Acid	0.000	0.009
Amides	0.000	0.000
HESim (Imide)	0.000	0.000
<b>HEP</b>	<b>0.713</b>	<b>0.830</b>
HEBA	0.000	0.000
<i>N</i> -methyl-...	0.058	0.006
<i>N</i> -ethyl-...	0.020	0.028
2-pyrrolidone	0.010	0.014
<i>N</i> -ethyl-pyrrolidine	0.007	0.000
Reduction only <sup>a</sup>	0.044	0.031
Oligomer <sup>b</sup>	0.148	0.082

<sup>a</sup> includes products such as  $\gamma$ -butyrolactone, 1,4-butanediol and butyric acid. <sup>b</sup> unidentified fraction of organics as determined from comparing HPLC with Karl-Fischer titration.

The main text mostly discusses differences in catalyst activity, which are suitably investigated at low conversion levels. However, high conversion scenarios are of greater industrial relevance and give additional information on consecutive side-reactions. Thus, the Pt-Re/TiO<sub>2</sub> (LD)

catalysts was compared to the Ru/C benchmark after prolonged reaction (**Table S1**). It is noted that the bimetallic catalyst yields a higher final amount of the target product HEP. This is due to reduced levels of (i) overreduction, e.g. *N*-methyl-2-pyrrolidone, and (ii) oligomer formation. Other authors<sup>[6, 7]</sup> have previously discussed the role of HEBA in oligomer formation. It is thus likely, that the reported performance of Pt-Re/TiO<sub>2</sub> (LD) is linked to its improved selectivity towards C-O hydrogenolysis as compared to the Ru/C benchmark.

#### 4. Heterogeneous Nature of the Catalyst

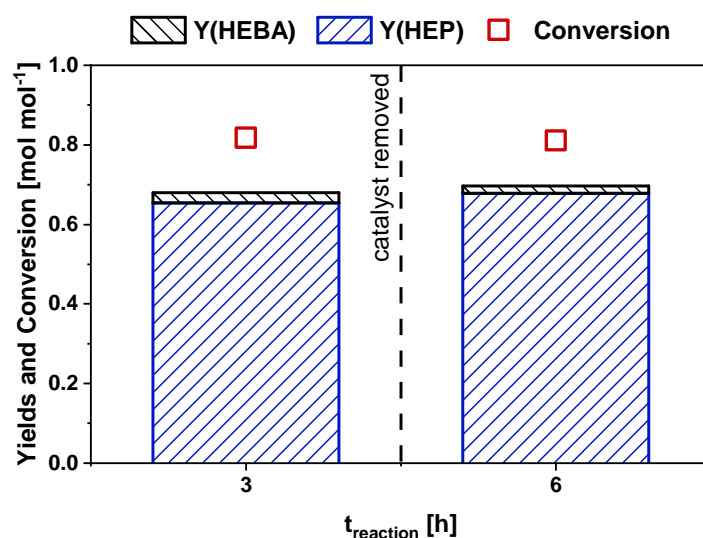


**Figure S4:** Hot filtration experiment using Pt-Re/TiO<sub>2</sub> (LD). (Conditions: 200 °C, 150 bar H<sub>2</sub>, 750 rpm, recipe of HESim reduction from main text scaled to 50 mg of catalyst)

The heterogeneous nature of the catalyst was tested by way of a hot filtration experiment (**Figure S4**). A typical HESim reduction reaction on Pt-Re/TiO<sub>2</sub> (LD) was interrupted after 3 h (batch mode) by cooling the autoclave to just below 100 °C. Subsequently, the vessel was

depressurized and opened, allowing for the removal of solids by filtration. The clear liquid was transferred back to the autoclave, followed by pressurization and heating to reaction temperature. A final sample was taken 3 h thereafter. From the respective results it is evident that the reaction had stopped after solids removal.

## 5. CSTR Catalyst Testing (Supplement)

**Table S2:** Detailed reaction data from CSTR operation at different conditions. (Conditions 10 h: 200 °C, 70 bar H<sub>2</sub>; Conditions 24 h: 220 °C, 100 bar H<sub>2</sub>)

Substrate/Product (i)	$n_i/n_{\text{substrate},0}$ [mol mol <sup>-1</sup> ]	
	10 h	24 h
Succinic Acid	0.179	0.108
Amides	0.058	0.051
HESim (Imide)	0.366	0.289
<b>HEP</b>	<b>0.269</b>	<b>0.343</b>
HEBA	0.027	0.035
<i>N</i> -methyl-...	0.000	0.018
<i>N</i> -ethyl-...	0.016	0.027
2-pyrrolidone	0.007	0.017
<i>N</i> -ethyl-pyrrolidine	0.000	0.000
Reduction only <sup>a</sup>	0.012	0.018
Oligomer <sup>b</sup>	0.066	0.094

<sup>a</sup> includes products such as  $\gamma$ -butyrolactone, 1,4-butanediol and butyric acid. <sup>b</sup> unidentified fraction of organics as determined from comparing HPLC with Karl-Fischer titration.

Pt-Re/TiO<sub>2</sub> (LD) was tested in a continuous stirred tank reactor (CSTR). In this context, selectivity and product yield were affected by the severity of operation conditions (**Table S2**). Higher temperature and hydrogen pressure sped up substrate conversion while also favoring the

formation of side-products. Especially, *N*-ethyl- and *N*-methyl-2-pyrrolidone from sequential HEP hydrogenation were increasingly detected. This highlights the main drawback of a CSTR setup, which operates under output conditions, i.e. at modest to high product concentrations in the entire reaction volume.

## 6. XRD Analysis (Supplement)

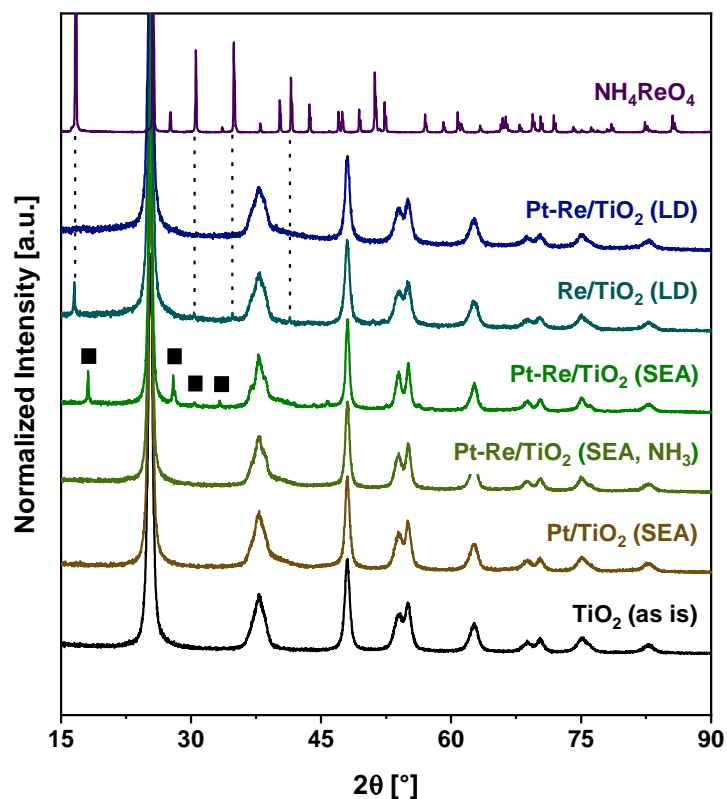


**Figure S5:** Powder XRD patterns of SEA and LD catalysts as compared to pure TiO<sub>2</sub> (anatase) and NH<sub>4</sub>ReO<sub>4</sub>. (■) indicates reflections tentatively assigned to an Na<sub>y</sub>ReO<sub>x</sub> phase formed with residual sodium from the SEA impregnation solution.

The XRD analysis of the main text is focused on Pt and Re/ReO<sub>x</sub> as likely active phases. Yet, some additional signals (**Figure S5**) were found for the monometallic parent of Pt-Re/TiO<sub>2</sub> (LD)

and for Pt-Re/TiO<sub>2</sub> (SEA). For Re/TiO<sub>2</sub> (LD), these reflections are immediately assignable to NH<sub>4</sub>ReO<sub>4</sub> remnants from precursor decomposition. In the case of Pt-Re/TiO<sub>2</sub> (SEA) the assignment is less straightforward. Yet, the absence of similar signals for Pt/TiO<sub>2</sub> (SEA) as well as for an analogue of Pt-Re/TiO<sub>2</sub> (SEA) prepared with NH<sub>3</sub> as a base for impregnation pH adjustments, suggests the joint presence of Na and Re as a source. While the few published structures of Na<sub>y</sub>ReO<sub>x</sub> do not yield an immediate match, additional reflections (■) are thus attributed to small quantities of a similar phase. Due to comparable catalytic behavior of Pt-Re/TiO<sub>2</sub> (SEA) catalysts synthesized with different bases (not shown), the role of Na<sub>y</sub>ReO<sub>x</sub> in HESim reduction is deemed negligible.

## 7. TEM Analysis (Supplement)

Particle sizes on monometallic Pt/TiO<sub>2</sub> catalysts (WI and SEA) were compared via HAADF-STEM (**Figure S6**). Both materials show spherical nanoparticles in the 2-3 nm size regime. While particles on the Pt/TiO<sub>2</sub> (WI) catalyst seem to be slightly smaller, this material also shows large Pt agglomerates (>10 nm, yellow circles) in the overview image. These are not accounted for in the particle count and are hard to quantify in a statistically sound way from TEM images. However, the comparison with other analysis techniques (e.g. XRD, CO-chemisorption) in the main text (Figure 6 and Table 3) shows that the SEA technique leads to an overall improvement in Pt utilization.

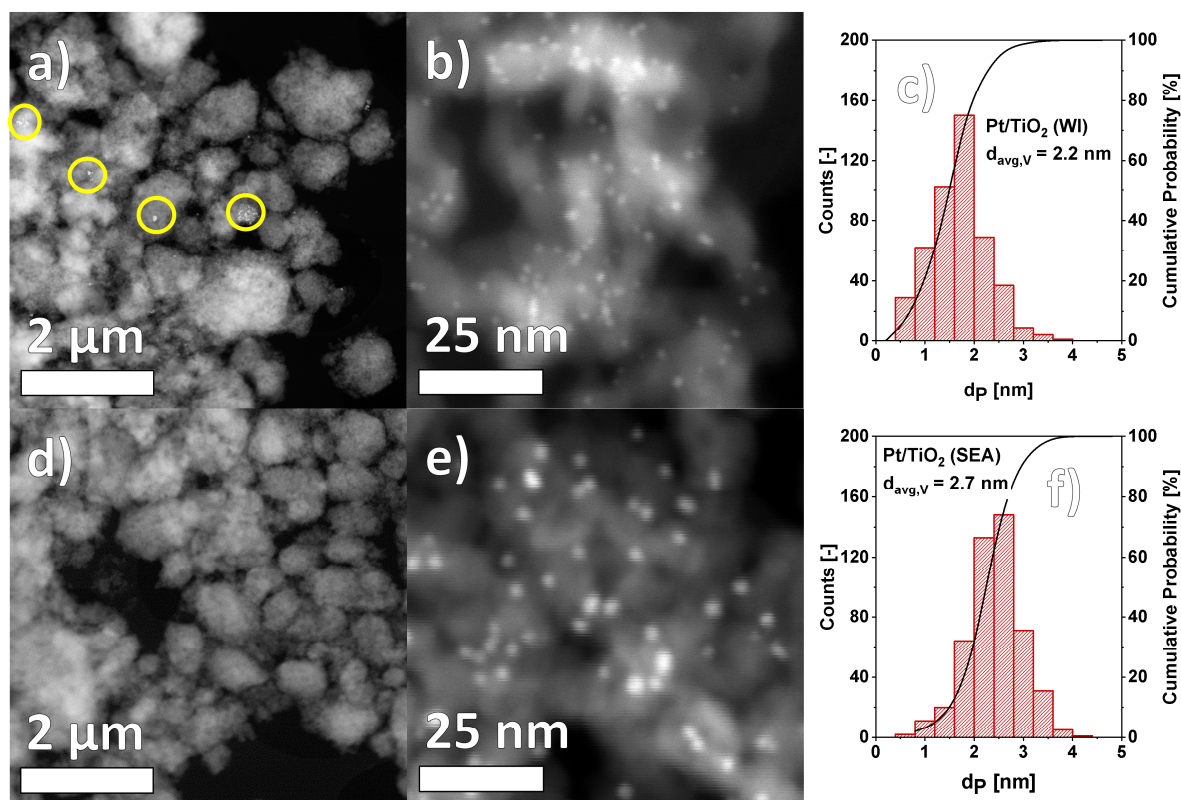


**Figure S6:** HAADF-STEM analysis of a-c) Pt/TiO<sub>2</sub> (WI) and d-f) Pt/TiO<sub>2</sub> (SEA).  $d_{\text{avg},V}$  is the volume-average particle diameter. Yellow circles highlight areas with large Pt agglomerates in the overview images. These are not incorporated into the particle count.

The monometallic Re/TiO<sub>2</sub> (LD) parent was also investigated (**Figure S7**). Some Re agglomerations were clearly visible in HAADF-STEM and might be associated with leftover NH<sub>4</sub>ReO<sub>4</sub> after thermal decomposition (see section 6, XRD). Moreover, Re was detected by EDX on several areas of the TiO<sub>2</sub> support that were optically free of particles giving notable z-contrast. It follows that at least some Re is spread over and functionalizes the TiO<sub>2</sub> surface, as is discussed in the main text.

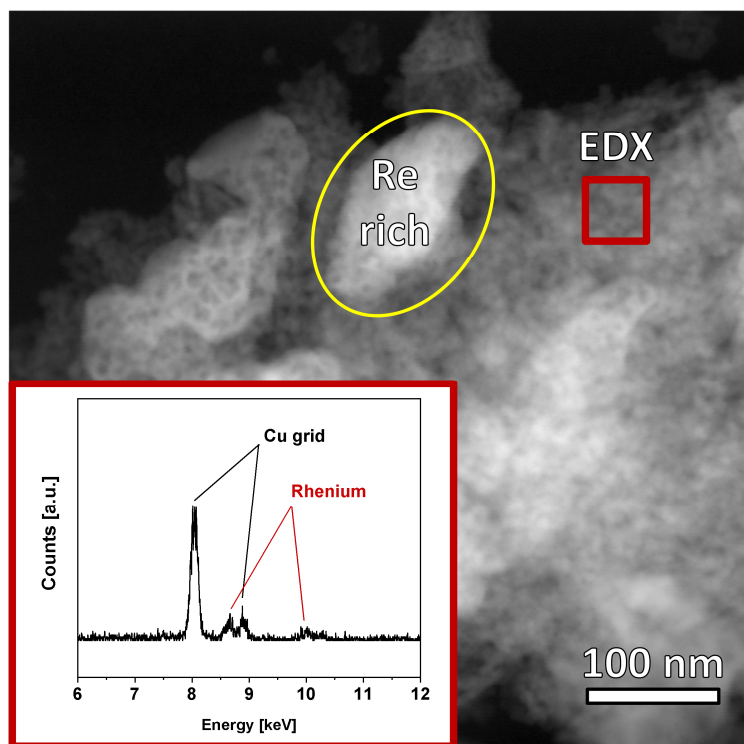


**Figure S7:** HAADF-STEM image and EDX analysis of the Re/TiO<sub>2</sub> (LD) parent material. The yellow circle highlights Re agglomeration, whereas the red square signifies the area of EDX analysis.

This is in line with high-magnification HAADF-STEM images of bimetallic Pt-Re/TiO<sub>2</sub> (x) catalysts (**Figure S8**). Next to the previously discussed nanoparticles, small clusters of metal atoms (< 1 nm) are visible. Since these are mostly observed on materials with high Re loading (a-c), and not on Pt-Re/TiO<sub>2</sub> (CR) (d), the small clusters are likely to be enriched in rhenium. Their size is not sufficient for the evolution of long-range order, which explains the absence of Re/ReO<sub>x</sub> XRD diffractions even at 10 wt % Re loading (Pt-Re/TiO<sub>2</sub> (LD)). While ReO<sub>x</sub> on the support likely influences sequential Pt impregnation (see main text, section 5), the observation of small metal clusters may have broader significance. In detail, metal clusters and single atoms are gaining increasing scientific attention and may influence the catalytic performance, even of

materials, which were previously considered as nanoparticulate.<sup>[8,9]</sup> In this context, a dedicated study into small Re (and Pt) clusters on TiO<sub>2</sub>-supported hydrogenation catalysts may be rewarding.

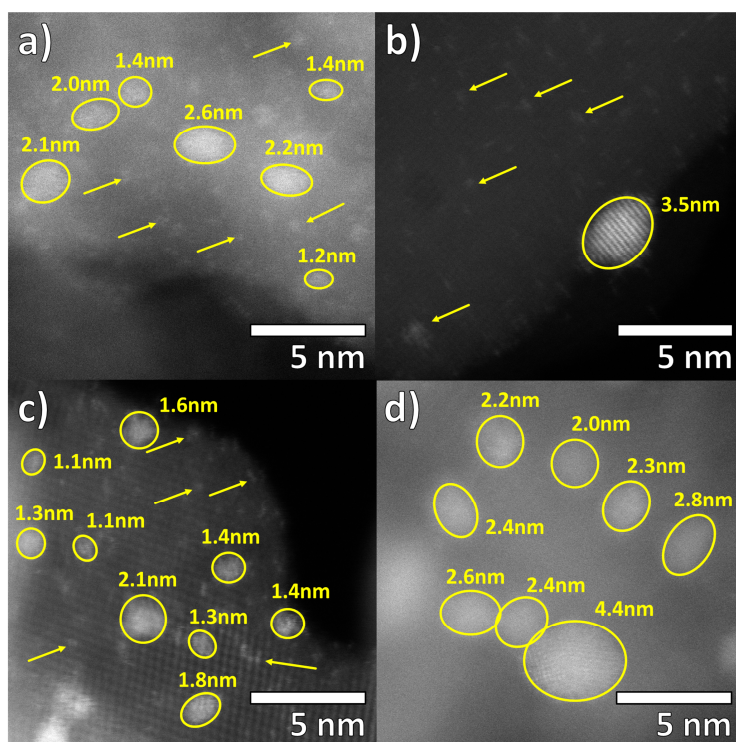


**Figure S8:** High-magnification HAADF-STEM images of Pt-Re/TiO<sub>2</sub> (x) catalyst samples. a) Pt-Re/TiO<sub>2</sub> (LD), b) Pt-Re/TiO<sub>2</sub> (SEA), c) Pt-Re/TiO<sub>2</sub> (CI), d) Pt-Re/TiO<sub>2</sub> (CR). Circles and arrows indicate metal nanoparticles and small clusters, respectively.

Lastly, the crystallinity of nanoparticles (< 5 nm) in Pt-Re/TiO<sub>2</sub> has been investigated by SAED (selected area electron diffraction, **Figure S9**). Interestingly, features of crystalline Pt (diffractions and lattice planes) were not observed for several of the bimetallic materials (Pt-Re/TiO<sub>2</sub> (LD) and (CI)). This is in line with the attribution of distinct Pt XRD reflections to large metal agglomerates, which were not evident in the sample sections chosen for SAED (see main text, section 4.1). While these contemplations exceed the focus of this work, it should be noted

that Re and  $\text{ReO}_x$  may affect Pt crystallization. Defect density may thus be another feature that distinguishes Pt-Re/ $\text{TiO}_2$  from pure Pt/ $\text{TiO}_2$  hydrogenation catalysts.

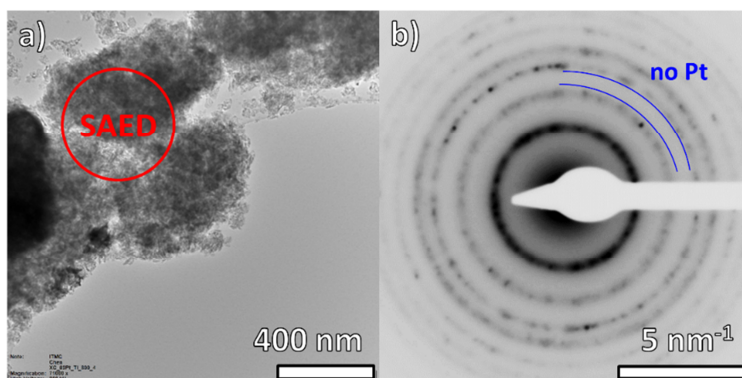


**Figure S9:** Exemplary SAED investigation of Pt-Re/ $\text{TiO}_2$  (LD). a) bright-field TEM with SAED aperture selection (red circle), b) SAE diffraction pattern with indications for the absence of primary Pt signals (blue lines).

## 8. XPS Analysis (Supplement)

**Figure S10** shows Pt XP spectra of several catalysts employed for HESim reduction. While the monometallic reference Pt/ $\text{TiO}_2$  (WI) shows a typical (asymmetric) peak shape, Pt4f<sub>7/2</sub> and Pt4f<sub>5/2</sub> contributions in bimetallic Pt-Re materials are represented by GL(30) profile functions. Combined with the shift in BE, this is indicative of Pt-Re interaction, possibly due to Re deposition on top of Pt surfaces.<sup>[10, 11]</sup> XPS fitting parameters associated with the evaluation of Pt and Re4f regions are documented in **Table S3**.

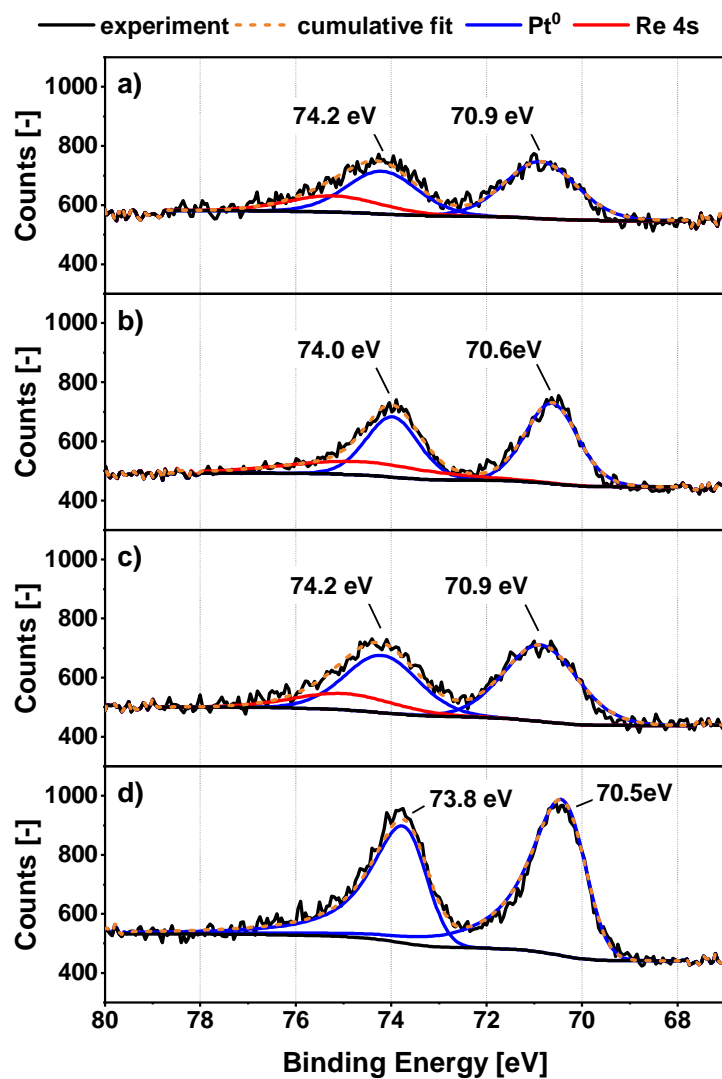


**Figure S10:** Pt4f region of several XP spectra collected with Pt-Re/TiO<sub>2</sub> (x) catalysts and reference materials. a) Pt-Re/TiO<sub>2</sub> (LD), b) Pt-Re/TiO<sub>2</sub> (SEA), c) Pt-Re/TiO<sub>2</sub> (CI) and d) Pt/TiO<sub>2</sub> (WI).

**Table S3:** Parameters used in the fitting of Pt and Re4f regions of XP spectra. Listed values correspond to 4f<sub>7/2</sub> signals, since 4f<sub>5/2</sub> contributions were fixed by  $\Delta$ BE and FWHM relations.

The chosen *in situ* reduction temperatures are given for clarity.

Species	Material	Pos. 4f <sub>7/2</sub> [eV]	FWHM [eV]
Pt <sup>0</sup>	Pt-Re/TiO <sub>2</sub> (LD), 150°C	70.9	1.8
	Pt-Re/TiO <sub>2</sub> (SEA), 150°C	70.6	1.3
	Pt-Re/TiO <sub>2</sub> (CI), 150°C	70.9	1.8
	Pt/TiO <sub>2</sub> (WI), 150°C	70.5	1.4
Re <sup>4+</sup>	Pt-Re/TiO <sub>2</sub> (LD), 150°C	42.0	1.7
	Pt-Re/TiO <sub>2</sub> (SEA), 150°C	42.1	1.5
	Pt-Re/TiO <sub>2</sub> (CI), 150°C	42.1	1.7
	Re/TiO <sub>2</sub> (WI), 150°C	42.0	1.4
	Re/TiO <sub>2</sub> (WI), 350°C	41.5	1.6
Re <sup>6+</sup>	Pt-Re/TiO <sub>2</sub> (LD), 150°C	43.0	1.7
	Pt-Re/TiO <sub>2</sub> (SEA), 150°C	42.8	1.7
	Pt-Re/TiO <sub>2</sub> (CI), 150°C	43.0	1.9
	Re/TiO <sub>2</sub> (WI), 150°C	43.4	1.9
	Re/TiO <sub>2</sub> (WI), 350°C	42.9	1.6
Re <sup>7+</sup>	Pt-Re/TiO <sub>2</sub> (CI), 150°C	45.8	1.5
	Re/TiO <sub>2</sub> (WI), 150°C	45.6	1.3
	Re/TiO <sub>2</sub> (WI), 350°C	45.7	1.0

## 9. CO-FTIR (Supplement)

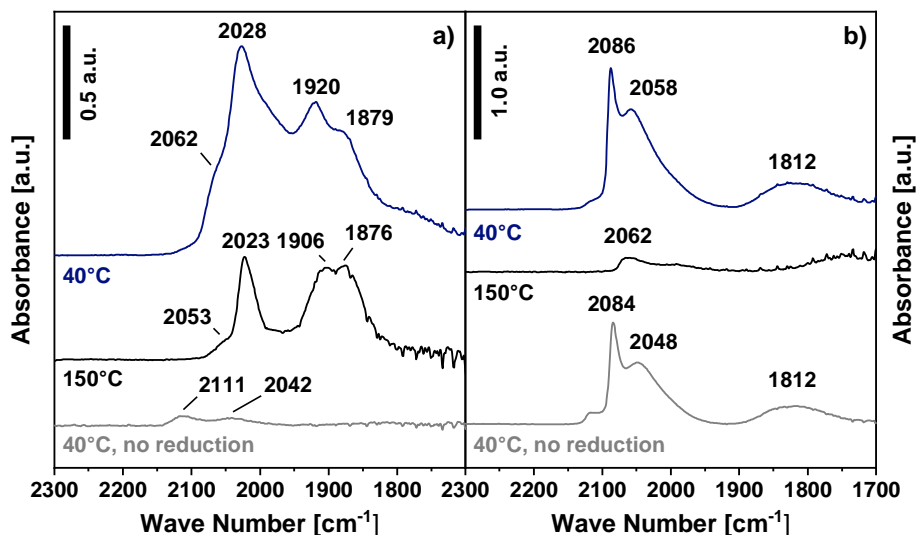


**Figure S11:** CO-FTIR spectra of a) Pt-Re/TiO<sub>2</sub> (LD) and b) Pt/TiO<sub>2</sub> (WI). Results from different desorption temperatures (40 and 150 °C) are compared to experiments without the *in situ* reduction step in sample pretreatment (“40 °C, no reduction”). Spectra are presented after baseline subtraction, without scaling.

The main text discussed the CO-FTIR spectra of several mono- and bimetallic catalysts. Bands at 2062 and 1794 cm<sup>-1</sup> as well as the red-side shoulder of the 2028 cm<sup>-1</sup> peak were attributed to CO adsorption on Pt. Signals centered at 2028, 1920 and 1878 cm<sup>-1</sup>, on the other hand, were associated with the formation of Re carbonyl. This distinction of two sets of bands becomes even more apparent during desorption experiments. Heating to 150 °C in flowing He (50 ml min<sup>-1</sup>) leads to the nigh disappearance of signals associated with Pt-CO (**Figure S11a**). Bands associated with Re carbonyl undergo a milder reduction and are thus dominant in the 150 °C spectrum. Notably, this is in line with CO desorption from monometallic Pt/TiO<sub>2</sub> (WI), which was almost complete in a similar experiment at 150 °C (**Figure S11b**). It also agrees with the previously reported temperature-stability of some Re carbonyl species.<sup>[12]</sup> Moreover, all bands

are slightly red-shifted at higher temperature, possibly due to thermal activation of the C-O bond and reduced CO surface coverage.

Lastly, the CO adsorption on Pt-Re/TiO<sub>2</sub> (LD) and Pt/TiO<sub>2</sub> (WI) was also compared in experiments without *in situ* reduction of the catalyst in the FTIR measurement cell. This led to a modest reduction in band intensity for Pt/TiO<sub>2</sub> (WI), which might even be attributed to sample thickness variations.<sup>1</sup> For Pt-Re/TiO<sub>2</sub> (LD), on the other hand, almost no CO adsorption was observed on the dried material. Moreover, the positions of the recorded low-intensity bands did not match observations with the reduced material. Thus, the reduction of rhenium species in the vicinity of Pt surfaces seems to have an impact on the formation of Pt-CO bands.

## 10. Solvent-Effect on HESim Reduction

A pronounced solvent-effect has been reported for hydrogenation reactions with Pt-Re/TiO<sub>2</sub> catalysts.<sup>[13]</sup> However, most literature systems operate in dilute substrate solutions with organic solvents. **Figure S12** thus shows the effect of changing solvent in dilute (1 mol L<sup>-1</sup>) conditions. Both 2MTHF and DME lead to substantially reduced conversion as compared to the aqueous system. These solvents also shift the balance of C-N vs. C-O hydrogenation in an unfavorable direction and are therefore less suitable in the current example. The observed solvent-effects can have several origins, including changes in metal reduction and substrate/product adsorption/desorption. A detailed distinction is not possible at this stage. Lastly, a comparison of

---

<sup>1</sup> Wafers for experiments with and without reductive pretreatment have been prepared separately. While the same mass of catalyst and KBr has been used in all cases, slight variations between samples cannot be excluded.

concentrated and dilute aqueous conditions indicates a reaction of zero order with respect to the imide substrate ( $n(\text{substrate}) \approx 0$ ). This is in line with earlier reports for the Ru/C system.<sup>[5]</sup>

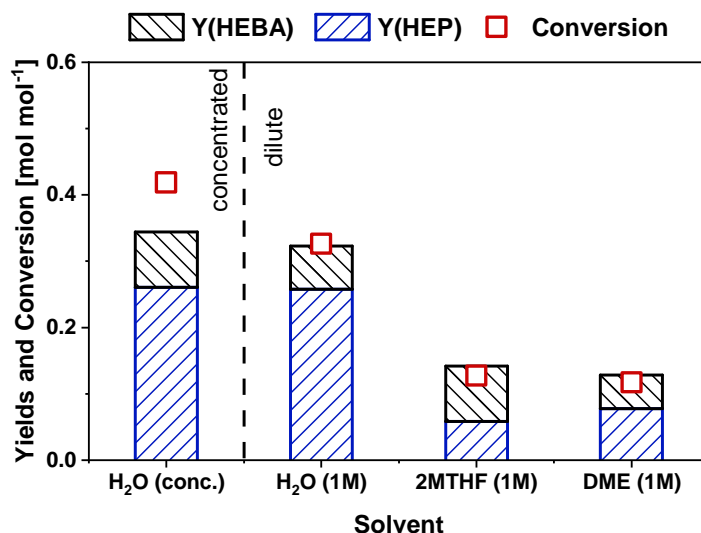


**Figure S12:** Solvent-effect in HESim hydrogenation over Pt-Re/TiO<sub>2</sub> (LD). Substrate dilution is achieved by variations in the amount of solvent whilst keeping the substrate/catalyst ratio constant (see recipe for HESim reduction, main text). (Conditions: 150 °C, 150 bar H<sub>2</sub>, 750 rpm, 1.5 g of dry MS 4Å for organic solvents)

## 11. Pressure-Dependence of HESim Hydrogenation

Other authors<sup>[14]</sup> have given an active site hypothesis for Pd-Re/SiO<sub>2</sub>. They found that activated H<sub>2</sub> plays a role in the rate-determining step and underlined this statement with the pressure-dependence of the investigated reduction. For Pt-Re/TiO<sub>2</sub> (LD)  $n(p(\text{H}_2))$  is likewise found to be around unity (**Figure S13**), indicating that hydrogen activation/activated hydrogen plays an important role. We would add that this allows for several explanations. For example,

Pt-promoted Re reduction may play a role in the catalytic cycle. Alternatively, as proposed by Takeda et al.,<sup>[14]</sup> H<sub>2</sub> activated by heterolytic dissociation on Pt-ReO<sub>x</sub> may be needed for efficient C=O reduction.

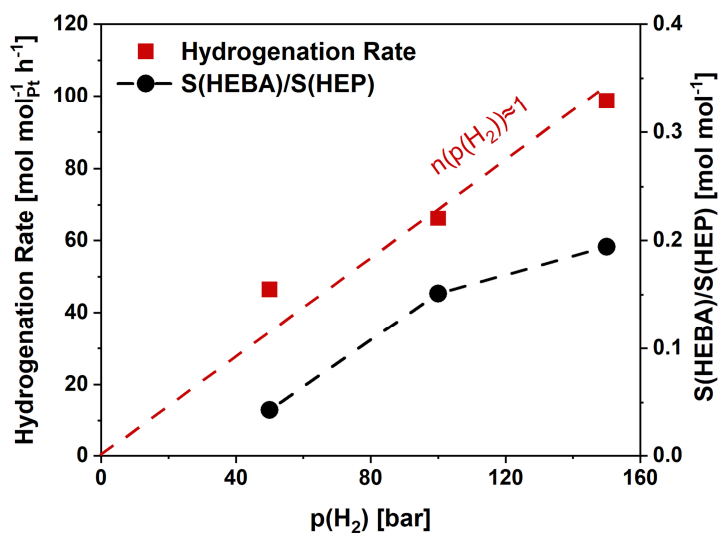


**Figure S13:** Pressure-dependence of HESim hydrogenation over Pt-Re/TiO<sub>2</sub> (LD). (Conditions: 150 °C, 50-150 bar H<sub>2</sub>, 750 rpm)

## 12. Dynamics of Pt-Re/TiO<sub>2</sub> Catalysts

It should be noted that the catalysts of this work could only be investigated at reaction temperature in a controlled gas phase environment. However, the presence of solvent (water) and higher H<sub>2</sub> pressure (50-150 bar) will also impact on their state during the reaction. In the presence of water or oxygen alone, the Re component of the catalyst would surely oxidize,<sup>[15, 16]</sup> leading to deactivation.<sup>[14]</sup> This is underlined by the necessity of protective atmosphere and organic solvents when working with monometallic Re reduction catalysts, which lack the

improved self-reduction properties provided by Pt.<sup>[17]</sup> Yet, the oxidizing effect of water is somewhat balanced by the presence of H<sub>2</sub>, making it difficult to reach a final conclusion. In this context, characterization of the spent catalyst (section 13) provides limited insight due to the adjustment of Pt-Re systems to their current environment.<sup>[18, 19]</sup>

Some evidence for an intermediate Re oxidation state in the active catalyst is provided by reactions in organic solvents in the presence of molecular sieve, which removes water from the reaction (**Figure S12**). These conditions, which would favor a more complete reduction and potentially even Pt-Re alloy formation,<sup>[20]</sup> lead to substantial reductions in catalyst activity. On the other hand, it has been shown that some extent of Re reduction proceeds even in humid atmosphere.<sup>[16]</sup> Together, these observations combine neatly with the identification of an intermediate reduction optimum for the activity of Re/TiO<sub>2</sub> hydrogenation catalysts.<sup>[17]</sup> Since this is circumstantial evidence, however, many research questions of interest remain in this field.

### **13. Characterization of Spent Catalyst**

A spent and deactivated catalyst sample (Pt-Re/TiO<sub>2</sub> (LD)) was collected after batch recycling (see main text, Figure 4). Its characterization by ICP-OES returned a lower Re content as compared to the fresh sample (**Table S4**). The reduced Re content was well in excess of the cumulative leaching of metal into the reaction solution (0.7 % relative  $\approx$  0.1 wt %; see main text, Figure 4). This gives further evidence for the role of catalyst washing in the recycle procedure, since the additional Re was likely leached at this stage. It follows that Pt-Re/TiO<sub>2</sub> (x) catalysts, whilst being comparably resistant towards leaching in reducing atmosphere (see also CSTR experiments, Figure 5), are prone to corrosion once exposed to oxygen. Consequently, a fraction of Re on the catalyst becomes water-soluble. Pt, on the other hand, was found to resist leaching.

**Table S4:** ICP-OES elemental analysis of fresh and batch recycled Pt-Re/TiO<sub>2</sub> (LD).

material	w(Re) [wt %]	w(Pt) [wt %]
fresh	10.1	3.92
spent	8.14	3.94

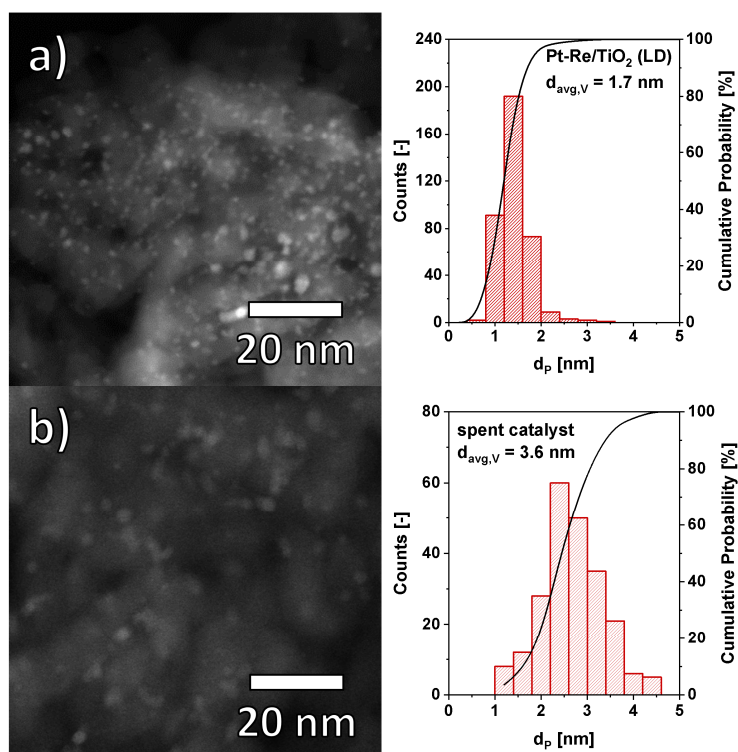


**Figure S14:** HAADF-STEM micrographs of a) fresh and b) batch recycled Pt-Re/TiO<sub>2</sub> (LD).  $d_{\text{avg,V}}$  is the volume-average diameter.

The same material was also subjected to TEM investigations, which showed that the average size of metal particles increased substantially in batch recycling (**Figure S14**). Thus, the observed decrease in catalyst activity will be due to a reduced number of active sites (see also Table 3, main text) and less Pt-Re interaction due to leaching. In this context, the latter may have an influence on the former since a role of Re in the inhibition of Pt sintering is discussed in

literature.<sup>[21, 22]</sup> It is noted that the presence of Re on TiO<sub>2</sub> is likely crucial in generating a well-dispersed metal phase in Pt-Re/TiO<sub>2</sub> (LD) in the first place (see main text, section 5).

Lastly, TPR gives additional evidence for reduced Pt-Re interaction in the spent catalyst (**Figure S15**). In detail, H<sub>2</sub> consumption features previously associated with Re reduction shifted by up to +35 °C as compared to the fresh material. It is therefore possible, that partial segregation of the two metals in a spent catalyst hampers their joint catalytic action in HESim reduction. However, the impact of organic adsorbates from the reaction stage also deserves contemplation.

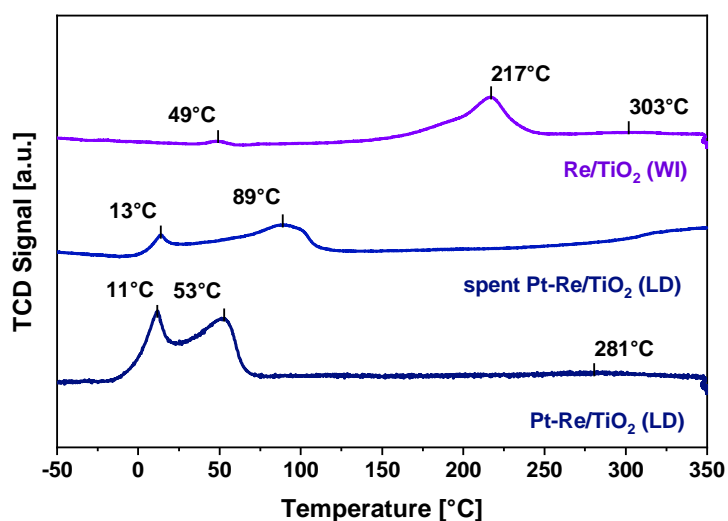


**Figure S15:** TPR profile of spent Pt-Re/TiO<sub>2</sub> (LD) as compared to the fresh material and Re/TiO<sub>2</sub> (WI). The spent sample was derived from CSTR operation and thus represents a case of comparably mild deactivation.

## 14. REFERENCES

- [1] J.S. Noh and J.A. Schwarz, Estimation of the point of zero charge of simple oxides by mass titration, *J. Colloid Interface Sci.* 130 (1989) 157-164. 10.1016/0021-9797(89)90086-6
- [2] J. Park and J.R. Regalbuto, A Simple, Accurate Determination of Oxide PZC and the Strong Buffering Effect of Oxide Surfaces at Incipient Wetness, *J. Colloid Interface Sci.* 175 (1995) 239-252. 10.1006/jcis.1995.1452
- [3] P. Wang, Aggregation of TiO<sub>2</sub> Nanoparticles in Aqueous Media: Effects of pH, Ferric Ion and Humic Acid, *Int. J. Environ. Sci. Nat. Res.* 5 (2017) 157-162. 10.19080/IJESNR.2017.01.555575
- [4] X. Hao, W.A. Spieker, J.R. Regalbuto, A further simplification of the revised physical adsorption (RPA) model, *J. Colloid Interface Sci.* 267 (2003) 259-264. 10.1016/S0021-9797(03)00644-1
- [5] M.O. Haus, Y. Louven and R. Palkovits, Extending the chemical product tree: a novel value chain for the production of *N*-vinyl-2-pyrrolidones from biogenic acids, *Green Chem.* 21 (2019) 6268-6276. 10.1039/c9gc01488h
- [6] Y. Shimasaki, H. Yano, H. Sugiura and H. Kambe, Development of a New Process for *N*-Vinyl-2-pyrrolidone, *Bull. Chem. Soc. Jpn.* 81 (2008) 449-459. 10.1246/bcsj.81.449
- [7] J.F. White, J.E. Holladay, A.A. Zacher, J.G. Frye Jr. and T.A. Werpy, Challenges in Catalytic Manufacture of Renewable Pyrrolidinones from Fermentation Derived Succinate, *Top. Catal.* 57 (2014) 1325-1334. 10.1007/s11244-014-0299-z

- [8] U. Petek, F. Ruiz-Zepeda, M. Bele and M. Gaberšček, Nanoparticles and Single atoms in Commercial Carbon-Supported Platinum-Group Metal Catalysts, *Catalysts* 9 (2019). 10.3390/catal9020134
- [9] L. Liu, M. Meira, R. Arenal, P. Concepcion, A.V. Puga and A. Corma, Determination of the Evolution of Heterogeneous Single Metal Atoms and Nanoclusters under reaction Conditions: Which Are the Working Catalytic Sites?, *ACS Catal.* 9 (2019) 10626-10639. 10.1021/acscatal.9b04214
- [10] A. Ramstad, F. Strisland, S. Raan, T. Worren, A. Borg and C. Berg, Growth and alloy formation studied by photoelectron spectroscopy and STM, *Surf. Sci.* 425 (1999) 57-67. 10.1016/S0039-6028(99)00185-5
- [11] A.S. Duke, R.P. Gallenge, S.A. Tenney, P. Sutter and D.A. Chen, *In Situ* Studies of Carbon Monoxide Oxidation on Platinum and Platinum-Rhenium Alloy Surfaces, *J. Phys. Chem.* 119 (2015) 381-391. 10.1021/jp509725n
- [12] F. Solymosi and T. Bánsági, CO-Induced Changes in Structure of Supported Rhenium, *J. Phys. Chem.* 96 (1992) 1349-1355. 10.1021/j100182a061
- [13] R. Burch, C. Paun, X.-M. Cao, P. Crawford, P. Goodrich, C. Hardacre, P. Hu, L. McLaughlin, J. Sá and J.M. Thompson, Catalytic hydrogenation of tertiary amides at low temperatures and pressures using bimetallic Pt/Re-based catalysts, *J. Catal.* 283 (2011), 89-97. 10.1016/j.jcat.2011.07.007
- [14] Y. Takeda, M. Tamura, Y. Nakagawa, K. Okumura and K. Tomishige, Characterization of Re-Pd/SiO<sub>2</sub> Catalysts for Hydrogenation of Stearic Acid, *ACS Catal.* 5 (2015) 7034-7047. 10.1021/acscatal.5b01054

- [15] M.T. Greiner, T.C.R. Rocha, B. Johnson, A. Klyushin, A. Knop-Gericke and R. Schlögl, The Oxidation of Rhenium and Identification of Rhenium Oxides During Catalytic Partial Oxidation of Ethylene: An In-Situ XPS Study, *Z. Phys. Chem.* 228 (2014) 521-541. 10.1515/zpch-2014-0002.
- [16] K. Lee, M.-E. Lee, J.-K. Kim, B. Shin and M. Choi, Single-step hydroconversion of triglycerides into biojet fuel using CO-tolerant PtRe catalysts supported on USY, *J. Catal.* 379 (2019) 180-190. 10.1016/j.jcat.2019.09.043
- [17] T. Toyao, K.W. Ting, S.M.A.H. Siddiki, A.S. Touchy, W. Onodera, Z. Maeno, H. Arigamiwa, Y. Kanda, K. Asakura and K.-I. Shimizu, Mechanistic study of the selective hydrogenation of carboxylic acid derivatives over supported rhenium catalysts, *Catal. Sci. Technol.* 9 (2019), 5413-5424. 10.1039/c9cy01404g
- [18] A.G.T.M. Bastein, F.J.C.M. Toolenaar and V. Ponec, Adsorption of Carbon Monoxide on Platinum Alloys: An Infrared Investigation, *J. Catal.* 90 (1984) 88-95. 10.1016/0021-9517(84)90088-5
- [19] A.S. Duke, R.P. Galhenage, S.A. Tenney, S.C. Ammal, A. Heyden, P. Sutter and D.A. Chen., *In Situ* Ambient Pressure X-ray Photoelectron Spectroscopy Studies of Methanol Oxidation on Pt(111) and Pt–Re Alloys, *J. Phys. Chem. C* 119 (2015) 23082-23093. 10.1021/acs.jpcc.5b07625
- [20] J. Sá, C. Kartusch, M. Makosch, C. Paun, J.A. van Bokhoven, E. Kleymenov, J. Szlachetko, M. Nachtgeal, H.G. Manyar and C. Hardacre, Evaluation of Pt and Re oxidation state in a pressurized reactor: difference in reduction between gas and liquid phase, *Chem. Commun.* 47 (2011), 6590-6592. 10.1039/C1CC10895F

[21] a) H. Iida and A. Igarashi, Difference in the reaction behavior between Pt-Re/TiO<sub>2</sub> (Rutile) and Pt-Re/ZrO<sub>2</sub> catalysts for low-temperature water gas shift reactions, *Appl. Catal., A* 303 (2006) 48-55. 10.1016/j.apcata.2006.01.029 b) H. Iida and A. Igarashi, Characterization of a Pt/TiO<sub>2</sub> (rutile) catalyst for water gas shift reaction at low-temperature, *Appl. Catal., A* 298 (2006) 152-160. 10.1016/j.apcata.2005.09.032

[22] J. Xiao and R.J. Puddephatt, Pt-Re clusters and bimetallic catalysts, *Coord. Chem. Rev.* 143 (1995) 457-500. 10.1016/0010-8545(94)07008-8